AERODYNAMIC DAMPING AND THE SEISMIC RESPONSE OF HORIZONTAL AXIS WIND TURBINE TOWERS

V. Valamanesh[a], S.M. ASCE and A.T. Myers[b] M. ASCE

[a] *Graduate Research Assistant, Department of Civil and Environmental Engineering, 360 Huntington Ave, 400 Snell Engineering Center, Northeastern University, Boston, MA 02215, USA, valamanesh.v@husky.neu.edu*

[b] *Assistant Professor, Department of Civil and Environmental Engineering, 360 Huntington Ave, 400 Snell Engineering Center, Northeastern University, Boston, MA 02215, USA, atm@neu.edu*

Abstract

Aerodynamic damping has an important effect on the seismic response of Horizontal Axis Wind Turbines (HAWTs). Some researchers have estimated that aerodynamic damping in operational HAWTs is ~5% of critical in the fore-aft direction (i.e. perpendicular to the rotor and parallel to the prevailing wind). In most recent studies, dynamic analyses of HAWT towers under seismic loads have neglected aerodynamic damping, and this assumption has significant implications in the predicted seismic response. We present a closed-form solution for the aerodynamic damping of HAWTs responding dynamically in the fore-aft and side-to-side directions. The formulation is intended as a convenient method for structural earthquake engineers to include the effect of aerodynamic damping in the seismic analysis of HAWTs. The formulation is based on Blade Element Momentum theory and is simplified by assuming a rigid rotor subjected to steady and uniform wind oriented perpendicular to the rotor plane. We examine the impact of these simplifying assumptions with an analysis of the 1.5-MW baseline HAWT developed by the National Renewable Energy Laboratory (NREL). The analysis compares predictions from this formulation to those from FAST, an open source program developed by NREL, and the comparison shows a reasonable correlation. Finally, the influence of aerodynamic damping on the seismic response of a HAWT is demonstrated for a dynamic model and the practical implications of the results are discussed.

Keywords

Horizontal Axis Wind Turbine, Aerodynamic Damping, Blade Element Momentum Theory, FAST Simulation, Seismic Response

Introduction

The wind energy industry continues to grow quickly throughout the world. In 2012, worldwide wind energy nameplate capacity exceeded 250 GW, more than double that from only four years prior (WWEA 2012, WWEA 2013). Roughly 16% of this installed capacity is in the United States (WWEA 2013), of which 20% is generated from the seismically active west coast (DOE 2012). The predominant type of wind turbine is the three-bladed Horizontal Wind Axis Turbine (HAWT). Other countries with significant seismic hazard, such as China and India, are quickly expanding their wind energy production capacity.

The seismic response of HAWTs is a topic that has only been studied recently and is increasingly important as the wind energy industry becomes an increasing source of worldwide energy generation. The seismic response is influenced by aerodynamic damping and the magnitude of this effect varies with the direction of the response relative to the rotor plane and the operational conditions. Aerodynamic damping is an effect in which the velocity of a vibrating structure induces a change in aerodynamic forces which usually reduce the dynamic response of the structure. This effect depends on the velocity term in the equation of motion and is additive with traditional structural damping (Salzmann and Tempel, 2005).

Design guidelines for wind turbines have recently included recommendations for determining seismic loads, but lack explicit recommendations on aerodynamic damping. The current edition of the international design standard, IEC-61400-1 (2005), includes provisions for calculating required strengths under combined seismic and operational loads and recommends that the structural damping for wind turbines be 1% of critical damping, but makes no recommendation for considering aerodynamic damping. A recent recommended practice published jointly by the American Wind Energy Association and the American Society of Civil Engineers (ASCE 2011) recommends that seismic design spectra for non-operational turbines should be based on total damping equal to 1%, while design spectra for operational turbines should be based on total damping equal to 5% to account for aerodynamic damping. The recommended practice makes no distinction between aerodynamic damping in the fore-aft or side-to-side directions.

In the current study, we present a closed-form solution based on Blade Element Momentum (BEM) theory for estimating the magnitude of aerodynamic damping of a HAWT tower responding dynamically in the fore-aft and side-to-side directions. The derivation of the closed-form solution is based on several simplifying assumptions, most notably a rigid rotor and a steady, uniform wind oriented perpendicular to the rotor plane. Although more refined estimates of aerodynamic damping could be obtained using linearizations in HAWT-specific analysis software such as FAST (NWTC 2013), the authors believe that a closed-form solution is useful to structural engineers who may be unfamiliar with HAWT-specific software and may prefer to accurately consider aerodynamic damping within software that has more refined structural analysis features.

The remainder of the paper is organized into five sections. First, background information on previous research into aerodynamic damping of HAWT towers and into the seismic response of HAWT towers is presented. This is followed by a derivation for the aerodynamic damping of an operational HAWT. The following section compares predictions from the derivation with those from FAST for the 1.5-MW baseline turbine developed by the National Renewable Energy Laboratory (Malcolm and Hansen 2002). This comparison includes an assessment of the impact of the simplifying assumptions on which the derivation is based. The next section demonstrates the influence of aerodynamic damping on the seismic response of a dynamic model of a HAWT tower and provides some practical interpretation of the results. In the final section, the key findings from this study are summarized.

Background

A few recent studies have examined the seismic response of HAWTs (Bazeos 2002, Witcher 2005, Prowell et al 2009, Nuta et al 2011), but most do not explicitly consider the influence of aerodynamic damping because most have considered non-operational, or parked, HAWTs, which are not strongly influenced by aerodynamic damping. Bazeos (2002) conducted dynamic finite element analyses to estimate the seismic response of a parked 450 kW HAWT tower. Lavassas et al (2003) investigated the

response of a 1-MW HAWT with 0.5% structural damping and no aerodynamic damping. Nuta et al (2011) assessed the seismic vulnerability of a parked 1.65-MW HAWT tower and did not consider aerodynamic damping. Witcher (2005) stated that operational wind turbines can experience total damping (aerodynamic plus structural) close to 5% and noted that, conveniently, this is commonly the same value prescribed by the seismic design spectra within many building codes.

Several prior studies have derived formulations for estimating aerodynamic damping of HAWT blades (Petersen et al 1998, Thomsen et al 2000, Hansen et al 2006 and Xiong et al 2010), but few studies have derived formulations of aerodynamic damping for HAWT towers. Some exceptions are work by Garrad (1990) and Kuhn (2001). Garrad derived aerodynamic damping for a HAWT with a rigid rotor and a flexible tower and Kuhn simplified the derivation by Garrad and formulated aerodynamic damping in terms of the derivative of the lift coefficient with respect to angle of the attack, geometric characteristics of the blades and dynamic characteristics of the tower. The derivation presented in this paper extends on these studies by including contributions to aerodynamic damping from the wind speed and by presenting equations for aerodynamic damping in the side-to-side direction. For the HAWT considered in the numerical example presented later, both effects are shown to contribute significantly to aerodynamic damping for some operational conditions.

Derivation of Aerodynamic Damping

The derivation for aerodynamic damping of an operational HAWT presented in this paper is based on a cantilever beam model of a HAWT tower with two degrees of freedom, lateral displacement at the hub height in the fore-aft (x-direction, perpendicular to the rotor plane) and side-to-side (y-direction, horizontal and within the rotor plane) directions. Fig. 1 shows a schematic of the model and defines the coordinate system and several geometric parameters used in the derivation. The figure shows a generic three-bladed HAWT with its rotor spinning at a rotational speed Ω and subject to a uniform upstream wind speed V_w in the fore-aft (x) direction. The figure also includes an image of a blade cross-section

located a radial distance r from the rotor hub. The cross-section is subjected to a relative wind velocity V_{rel} that is comprised of a component normal to the rotor plane $V_x = V_w(1-a)$, where a is the axial induction factor, and a component within the rotor plane $\Omega r(1+a')$, where a' is the tangential induction factor. The axial induction factor defines the wind speed at the rotor V_x relative to the upstream wind speed V_w and the tangential induction factor defines the ratio between the angular velocity imparted to the air flow after passing through the rotor and the rotational speed of the rotor (Manwell et al 2002). The relative wind on the cross-section induces lift and drag forces that can be decomposed into components in the fore-aft (F_x) and side-to-side (F_y) directions. The figure also defines the chord length c and several angles including the angle of attack α, the pitch angle β, and the angle of the relative wind ϕ.

For the derivation presented in this paper, the rotor blades are modeled as rigid and the mass of the rotor nacelle assembly and the equivalent modal mass of the tower are modeled as an equivalent mass m concentrated at the turbine hub. The tower is modeled as a cantilever beam with lateral stiffness k. The equations of motion for the fore-aft (x) and side-to-side (y) directions are provided below,

$$m\ddot{x} + c_{ST}\dot{x} + kx = dF_x \quad (1)$$

$$m\ddot{y} + c_{ST}\dot{y} + ky = dF_y \quad (2)$$

where c_{ST} is the structural damping coefficient and dF_x and dF_y are incremental changes in aerodynamic forces at the rotor hub induced by lateral motion. Aerodynamic forces are estimated based on Blade Element Momentum (BEM) theory (Glauert 1976). In the following sections, a derivation for estimating aerodynamic damping in the fore-aft direction is presented first and followed by a derivation for the side-to-side direction.

Aerodynamic Damping in the Fore-Aft Direction

The total aerodynamic force F_x acting at the hub of the rotor is equal to the aerodynamic force in the x-direction acting at each blade cross-section, integrated over the radial length of each blade and multiplied by the number of blades N_b in the rotor as shown below,

$$F_x = \frac{1}{2}\rho N_b \int [V_{rel}^2 [C_L \cos(\phi) + C_D \sin(\phi)] c(r)] dr \quad (3)$$

where ρ is the density of air, C_L and C_D are the coefficients of lift and drag for the blade, c is the chord length of the blade, and V_{rel}^2 is the square of the relative wind defined as,

$$V_{rel}^2 = V_x^2 + (\Omega r)^2 (1 + a')^2 \quad (4)$$

A rotor with a hub that is moving in the fore-aft direction with velocity $\dot{x}$ will experience a change in the relative fore-aft wind velocity between the rotor and the air, as shown in Eq. (5).

$$dV_x = V_w(1 - a) - \dot{x} \quad (5)$$

This change in the relative fore-aft wind velocity induces a change in the fore-aft aerodynamic force on the rotor dF_x. The relationship between dF_x and dV_x is provided below,

$$\frac{dF_x}{dV_x} = \frac{\partial F_x}{\partial V_x} + \frac{\partial F_x}{\partial \phi}\frac{d\phi}{dV_x} \quad (6)$$

where,

$$\frac{\partial F_x}{\partial V_x} = \rho N_b \int V_x [C_L \cos(\phi) + C_D \sin(\phi)] c(r) dr \quad (7)$$

$$\frac{\partial F_x}{\partial \phi} = \frac{1}{2}\rho N_b \int [V_{rel}^2 \left[\frac{\partial C_L}{\partial \phi}\cos(\phi) + \frac{\partial C_D}{\partial \phi}\sin(\phi) + C_D \cos(\phi) - C_L \sin(\phi)\right] c(r)] dr \quad (8)$$

$$\frac{d\phi}{dV_x} = \frac{\Omega r(1+a')}{V_{rel}^2} \quad (9)$$

Note that, because the variables ϕ and α differ by a constant, the derivatives of C_L and C_D with respect to ϕ are equivalent to the derivatives of C_L and C_D with respect to α. Eqs. (7)-(9) can be substituted into Eq. (6) and rearranged as in Eq. (10) below,

$$dF_x = N_b(A + B)dV_x \quad (10)$$

where A represents the portion of dF_x generated by the upstream wind V_w, see Eq. (11), and B represents the portion generated by Ω, see Eq. (12).

$$A = \rho \int V_w(1-a)[C_L \cos(\phi) + C_D \sin(\phi)]c(r)dr \quad (11)$$

$$B = \frac{1}{2}\rho \int \Omega r(1+a')\left[\left(\frac{\partial C_L}{\partial \alpha} + C_D\right)\cos(\phi) + \left(\frac{\partial C_D}{\partial \alpha} - C_L\right)\sin(\phi)\right]c(r)dr \quad (12)$$

Eqs. (5) and (10) can be substituted into Eq. (1) and, upon rearranging of terms, the equation of motion is expressed as,

$$m\ddot{x} + [c_{ST} + N_b(A+B)]\dot{x} + kx = N_b(A+B)V_w(1-a) \quad (13)$$

The damping in this equation is composed of two components, the structural damping c_{ST} and the aerodynamic damping c_{AD} which is defined in the equation as,

$$c_{AD} = N_b(A+B) \quad (14)$$

The aerodynamic damping ratio in the fore-aft direction $\xi_{AD,x}$ is provided in Eq. (15) and is a linear combination of two terms, one representing the effects of V_w, Eq. (11), and the other representing the effects of Ω, Eq. (12).

$$\xi_{AD,x} = \frac{c_{AD}}{2\sqrt{km}} = \frac{N_b(A+B)}{2\sqrt{km}} \quad (15)$$

Aerodynamic Damping in the Side-to-Side Direction

The HAWT shown schematically in Fig. 2 is similar to that in Fig. 1 but has a different perspective and shows that the rotor is subjected simultaneously to steady winds in both the fore-aft and side-to-side directions, represented by V_x and V_y, respectively. Wind turbines with active yaw systems are controlled to maintain the rotor plane perpendicular to the prevailing wind direction, thus, for most situations, the rotor can be expected to be perpendicular to the prevailing wind direction. Therefore, the derivation presented below is eventually simplified by assuming that the prevailing wind direction is perpendicular

to the rotor plane and that there is no wind in the side-to-side direction (i.e. $V_y = 0$). The impact of this assumption is assessed in the next section.

The total side-to-side aerodynamic force acting at the hub is provided below,

$$F_y = \frac{1}{2}\rho \sum_{i=1}^{N_b} \int V_{rel}^2 [C_L \sin(\phi) - C_D \cos(\phi)] c(r) \cos(\gamma_i(t)) dr \quad (16)$$

where $\gamma_i(t)$ is the azimuth angle of blade i and varies as a function of time t and

$$V_{rel}^2 = [V_x^2 + [\Omega r(1 + a') + V_y \cos(\gamma_i(t))]^2] \quad (17)$$

The incremental change in the side-to-side relative wind due to the dynamic response of the HAWT in this direction is provided in the equation below,

$$dV_y = V_y - \dot{y} \quad (18)$$

Following the same procedure as outlined in the previous section, and assuming $V_y = 0$, the change in the side-to-side aerodynamic force on the rotor dF_y is provided below,

$$dF_y = \sum_{i=1}^{N_b} (B' - A')[\cos(\gamma_i(t))]^2 \, dV_y \quad (19)$$

where A' represents the portion of dF_y generated by V_w and B' represents the portion generated by Ω.

$$A' = \frac{1}{2}\rho \int V_w (1 - a) \left[\left(\frac{\partial C_L}{\partial \alpha} + C_D \right) \sin(\phi) + \left(C_L - \frac{\partial C_D}{\partial \alpha} \right) \cos(\phi) \right] c(r) dr \quad (20)$$

$$B' = \rho \int \Omega r (1 + a') [C_L \sin(\phi) - C_D \cos(\phi)] c(r) dr \quad (21)$$

It can be shown that a symmetric HAWT with three blades will have the following property for any value of t,

$$\sum_{i=1}^{N_b} [\cos(\gamma_i(t))]^2 = \frac{N_b}{2} \quad (22)$$

Eqs. (18), (19) and (22) can be substituted into Eq. (2) and, upon rearranging terms, the equation of motion is expressed as,

$$m\ddot{y} + \left(c_{ST} + N_b \frac{B' - A'}{2}\right)\dot{y} + ky = 0 \tag{23}$$

The aerodynamic damping ratio in the side-to-side direction $\xi_{AD,y}$ is provided in Eq. (24) and is a linear combination of two terms, one representing the effects of V_w and the other representing the effects of Ω.

$$\xi_{AD,y} = \frac{N_b(B' - A')}{4\sqrt{km}} \tag{24}$$

Given the aerodynamic damping in the fore-aft and side-to-side directions of a HAWT, the aerodynamic damping in any direction can be obtained using a transformation matrix. A similar procedure has been proposed by Peterson to obtain aerodynamic damping of a blade in any direction (Peterson et al 1998).

Numerical Example – The 1.5-MW NREL Baseline HAWT

In the previous sections, equations for estimating the aerodynamic damping of a HAWT in the fore-aft and side-to-side directions were presented. The current section is divided into two parts, both of which consider the 1.5-MW baseline turbine developed by NREL (Malcolm and Hansen 2002). In the first part, results from the derivation are compared to those from FAST for the baseline turbine. The comparison is made under parked and operational conditions and the FAST results include predictions of the aerodynamic damping both with and without the assumptions inherent to the closed-form solution. In the second part, the relative importance of terms within the closed-form solution is examined to assess assumptions inherent to previous derivations (Garrad 1990, Kuhn 2001) which have assumed high tip speed ratios and thus have ignored contributions to aerodynamic damping from the wind speed.

The specifications of the 1.5-MW baseline turbine are provided in Table 1. Each blade of the baseline turbine is composed of three segments, each with a different airfoil designation: S818, S825 and S826 (NWTC 2013). All three airfoils have nearly the same drag and lift characteristics which are shown in

Fig. 3 for the S818 airfoil. The considered 1.5-MW turbine is a variable speed, variable pitch machine and so the pitch and rotor speed are controlled to optimize power output for any wind speed. For this turbine, the rated wind speed is 11.5 m/s. At wind speeds above this speed, the blade pitch increases while the rotor speed is held constant at the maximum speed, 20 rpm, to maintain rated power output. Below the rated wind speed, rotor speed decreases while blade pitch is held constant to maximize power output. For steady state conditions, the dependence of rotor speed and blade pitch on wind speeds between cut-in and cut-out is roughly as shown in Fig. 4. All results presented for operational conditions are based on combinations of wind speed, rotor speed, and blade pitch as specified in Fig. 4, while all results presented for parked conditions are based on a stationary rotor with feathered blades.

Verification of Aerodynamic Damping with FAST

To evaluate the proposed closed-form solution, a model of the 1.5-MW baseline wind turbine is analyzed with FAST under operational and parked conditions with and without many of simplifying assumptions inherent to the closed-form solution. Estimates from the closed-form solution are compared with results predicted by FAST for aerodynamic damping in the fore-aft and side-to-side directions. The FAST results are predicted at 21 different steady wind speeds, evenly spaced between cut-in and cut-out. The method to calculate aerodynamic damping in FAST starts with a model of the 1.5-MW baseline turbine with no structural damping so that all damping of the displacement response may be attributed to aerodynamic effects. This model is first subjected to a steady wind and then subjected to an impulse acceleration at the base of the model. Following the impulse, the decay of the displacement time history at the hub is recorded in the fore-aft and side-to-side directions and the magnitude of aerodynamic damping in each direction is calculated by applying the logarithmic decrement method (Chopra 2011) to the first and fourth peaks of the displacement time history. Seven FAST analyses, with varying degrees of simplification, are conducted at each wind speed to thoroughly investigate the accuracy of the closed-form solution. The features of each analysis are listed in Table 2. The first analysis is designed to most closely replicate realistic conditions, while the last analysis (#7) is designed to most closely replicate the

simplifying assumptions of the closed-form solution. The intermediate analyses are designed to investigate the impact of each simplifying assumption individually. It is important to emphasize that, although analysis #7 is intended to most closely resemble the assumptions of the closed-form solution, there still remain many differences between the formulation of FAST and the closed-form solution. For example, for the fore-aft and side-to-side directions, FAST considers two mode shapes which include the effects of distributed mass and stiffness, whereas the closed-form solution is based on an equivalent cantilever beam model with lumped mass at the hub. More importantly, the inflow model in FAST is based on the Generalized Dynamic Wake model (NWTC 2013) and considers many features not considered in the closed-form solution, which is based on Blade Element Momentum theory. For example, the inflow model in FAST considers the dynamic wake effect and losses at the hub and blade tips.

In Fig. 5, aerodynamic damping is estimated in the fore-aft direction based on Eq. (15) and on FAST for the seven analyses specified in Table 2. The estimates are provided as a function of wind speed for both parked and operational conditions. Overall, Eq. (15) gives a reasonable but generally lower estimate of aerodynamic damping compared to all seven FAST analyses. The agreement between results is strongest for parked conditions and for wind speeds greater than the rated wind speed. For operational conditions, the mean value of predictions per Eq. (15) is 4.6% and the range is between 3.7% and 5.4%. As seen in Fig. 5, for the range of analyses considered, the most influential assumption is that of a rigid rotor which tends to lower the estimates compared to those with a flexible rotor (Analyses #1 and #2). On average, the aerodynamic damping predictions from Analysis #1, the most realistic of the considered simulations, are 0.6% higher than those from Eq. (15) for operational conditions and nearly identical for parked conditions. Comparing the results from Eq. (15) with those from Analysis #7, which is designed to most closely replicate the simplifying assumptions of Eq. (15), shows that predictions based on Eq. (15) are, on average, 0.7% lower for operational wind speeds between cut-in and rated and 0.1% lower for operational wind speeds between rated and cut-out. For wind speeds between cut-in and rated, the FAST predictions

255 including pre-cone and wind shear are shown to have similar effects with predictions averaging 0.7%
256 higher than Eq. (15).

257 The assumption of a steady wind (i.e. no turbulence) is another important simplification of the closed-
258 form solution. To assess the impact of this simplification, Analysis #1 was repeated fifteen times with a
259 turbulent wind history and a mean wind speed equal to the rated wind speed. The turbulent history is
260 calculated based on the Normal Turbulence Model with a turbulence intensity of 0.15 (IEC 2005). For
261 this particular case, the aerodynamic damping in the fore-aft direction was estimated as 5.7% for steady
262 conditions and, for turbulent conditions, the mean and standard deviation of the fifteen simulations are
263 6.0% and 2.1%, respectively. It is further noted that, in an average sense, the plots of the displacement
264 response at the hub following the application of the impulse load for the steady and turbulent conditions
265 are nearly identical, except that the response for the turbulent conditions contains some small-amplitude,
266 high-frequency oscillations.

267 Fig. 6 is similar to Fig. 5, except that results are compared with FAST for aerodynamic damping in the
268 side-to-side direction. The results in Fig. 6 show that both Eq. (24) and the FAST analyses predict very
269 small magnitudes of aerodynamic damping in the side-to-side direction. At such small magnitudes of
270 aerodynamic damping, the effect of the differences between FAST and the closed-form solution are more
271 pronounced. Nevertheless, for all conditions considered, the aerodynamic damping predicted by both
272 FAST and Eq. (24) never exceeds 0.5%. For operational conditions, the mean value of aerodynamic
273 damping per Eq. (24) is 0.1% and the range is between ~0.0% and 0.3%.

274 ***Relative Importance of Terms in the Closed-form Solution***

275 The derivation presented in this paper does not assume that wind speed is negligible compared to rotor tip
276 speed, and the result is that the predicted aerodynamic damping depends on two components, the first,
277 presented in Eq. (11) and labeled component A, depends on the wind speed, and the second, presented in
278 Eq. (12) and labeled component B, depends on the rotor speed. Fig. 7 shows predictions of aerodynamic

damping in the fore-aft direction for the baseline turbine under parked and operational conditions. The figure shows that the component of the total aerodynamic damping that is attributed to the wind speed (A component) increases nearly linearly with increasing wind speed. At cut-in, 6.7% of the total damping is due to this term, while at cut-out, the proportion increases to 41%. The figure also includes a plot indicating the proportion of the rotor speed component of damping (B component) that is attributed to the derivative of the lift coefficient with respect to the angle of attack. This plot shows that the B component of damping is completely dominated by contributions from the lift coefficient derivative. The implication is that, for the considered turbine, predictions of aerodynamic damping will remain virtually unchanged if Eq. (12) is simplified to,

$$B = \frac{1}{2}\rho \int \Omega r(1 + a') \frac{\partial C_L}{\partial \alpha} \cos(\phi) c(r) dr \tag{25}$$

Influence of Aerodynamic Damping on the Seismic Response of a HAWT

The impact of aerodynamic damping on the seismic response of a HAWT is demonstrated using a dynamic model of the 1.5-MW baseline turbine. The model is an Euler-Bernoulli cantilever discretized by 11 nodes into 10 beam elements. Equivalent mass is concentrated at each node to represent the mass of the tower, nacelle and rotor. The total damping in the model is the sum of structural damping, assumed to be 1% of critical, and aerodynamic damping. The model is analyzed under 7 ground motion recordings selected from the Pacific Earthquake Engineering Research Center ground motion database using recommendations from FEMA 440 (2005) for soil type C. Details for these records are listed in Table 3. For the analyses considered here, each ground motion is scaled to match the design spectral acceleration following ASCE 7-10 for a site representative of a U.S. location with high seismic activity, specifically a spectral acceleration of 0.7g at a one second period for the maximum considered earthquake. For the baseline HAWT, which has a fundamental period of vibration of 2.5 s, the design spectral acceleration for this location, assuming 5% total damping, is 0.26 g. Each ground motion is applied as an acceleration boundary condition at the base of the structural model and a linear dynamic time history analysis is

303 conducted to characterize the seismic response of the structure. The dynamic analyses also include the
304 effects of aerodynamic thrust acting on the rotor in the fore-aft direction. The thrust is calculated in FAST
305 as a function of wind speed for a steady uniform wind under realistic operational conditions. The
306 magnitude of aerodynamic damping for each analysis is calculated as a function of wind speed based on
307 one of three methods: FAST, the closed-form solution, or a constant value. The aerodynamic damping
308 calculated by FAST is based on the conditions of Analysis #1 (see Table 2), but without wind shear.

309 The results of these analyses are provided in Fig. 8, which, for all seven ground motions, shows the
310 median spectral drift (i.e. the median lateral displacement at the hub divided by the hub height) as a
311 function of wind speed for parked and operational conditions. Results are organized as being in either the
312 fore-aft direction, in which case aerodynamic thrust adds to the drift caused by ground shaking, or in the
313 side-to-side direction, in which case there is no aerodynamic thrust. The component of the drift caused by
314 the seismic loading is reduced by a factor of 1.5 to reflect recommendations by ASCE (2011) that wind
315 turbine towers should be designed with a seismic modification factor of R = 1.5. In this way, the results
316 are intended to be similar to design conditions, which as specified by IEC (2005) and ASCE (2011),
317 should consider simultaneous operational and earthquake loads. It is important to note that, although not
318 considered here, an IEC compliant design would be required to consider additional loads such as gravity
319 loads, turbulence, or loads due to operational conditions such as an emergency stop of the rotor.

320 Overall, there is strong agreement between FAST and the closed-form solution. Moreover, for parked
321 conditions in both directions and operational conditions in the side-to-side direction, both models agree
322 strongly with results based on total damping equal to 1% and, for operational conditions in the fore-aft
323 direction, both models agree strongly with results based on total damping equal to 5%. Note that for
324 operational conditions in the fore-aft direction, results based on total damping equal to 1% are ~20%
325 larger than those based on FAST and those based on the closed-form solution. Thus, for the considered
326 1.5-MW turbine, reasonable approximations are that there is 1% total damping in the side-to-side
327 directions for all conditions, 1% total damping in the fore-aft direction for parked conditions, and 5% total

damping in the fore-aft direction for operational conditions. These approximations are aligned with the recommendations by ASCE (2011) which state that total damping should be set to 1% during parked conditions and 5% during operational conditions. It's important to note though that ASCE does not distinguish its recommendation for operational conditions based on direction.

For all three methods presented in Fig. 8, the largest median drifts occur in the fore-aft direction at the cut-out wind speed and have magnitudes slightly larger 0.8%. In the side-to-side direction, the median drift is ~0.5% regardless of the wind speed. As a frame of reference, for the 1.5-MW tower, a drift of 0.8% corresponds to a base moment equal to the yield moment, assuming the tower deforms in the shape of its first mode. When interpreting these results, it is important to remember that the intensity of the ground shaking was selected based on a design spectrum with 5% total damping. While this selection is reasonable for operational conditions in the fore-aft direction, it is not for operational conditions in the side-to-side direction which, more reasonably, should have been based a design spectrum with 1% total damping. This detail is important because, in some cases, it may cause the controlling design condition to shift from the fore-aft to the side-to-side direction, since a spectral acceleration at 1% damping is 1.4 times greater than that at 5% damping (ASCE 2011). A lower seismic modification factor, for example R = 1, could cause a similar shift. However, for the considered turbine and tower, an earthquake, scaled to a spectral acceleration representative of design conditions for a high-risk seismic location and applied simultaneously with the thrust at cut-out, is predicted to cause a base moment that exceeds the yield moment, given the modeling methods described previously.

Although results presented here for the 1.5-MW turbine are aligned with the recommendations of ASCE (2011), the magnitude of aerodynamic damping will change for different turbine types and sizes. For example, Prowell (2011) studied a 65-kW turbine under operational conditions at lower wind speeds (near cut-in) and experimentally measured aerodynamic damping in the fore-aft direction to be 1.0% of critical. Similarly, an analysis in FAST of the 5-MW baseline turbine developed by NREL, subjected to a steady

wind equal to the rated wind speed, predicts that aerodynamic damping in the fore-aft direction is 6.7% of critical, while the equivalent value for the 1.5-MW turbine is 6.1%.

Conclusions

The aerodynamic damping of an operational HAWT responding dynamically in the fore-aft and side-to-side directions is derived in closed-form based on Blade Element Momentum theory. The estimated results from the derivation are compared with those from FAST for the 1.5-MW baseline HAWT under parked and operational conditions and the comparison shows reasonable agreement. Under operational conditions and for the same turbine, the derivative of the lift coefficient of the blades with respect to the angle of the attack is shown to contribute most to aerodynamic damping, however, the contribution lessens as wind speeds approach the cut-out wind speed.

The aerodynamic damping in the fore-aft direction for the 1.5-MW turbine is estimated by the closed-form solution to be between 0.0% and 0.6% for parked conditions and between 3.7% and 5.4% under operational conditions. For the side-to-side direction, the estimates are ~0.0% for parked conditions and between ~0.0% and 0.3% for operational conditions. An analysis of the impact of some of the simplifying assumptions inherent to the derivation shows that the most influential assumption is that of a rigid rotor and that this assumption can reduce predictions of aerodynamic damping for operational conditions in the fore-aft direction by an average of ~1.0%.

The results from a linear dynamic model of the baseline HAWT subjected to seven ground motions and simultaneous aerodynamic thrust showed that the largest drift demands occurred in the fore-aft direction at the cut-out wind speed. For the considered turbine, a constant value of 5% total damping provides a reasonable estimate of the seismic response for operational conditions in the fore-aft direction while a constant value of 1% total damping provides a reasonable estimate of the seismic response for parked conditions in all directions and for operational conditions in the side-to-side direction. These estimates align well with recent recommendations from ASCE (2011), with the exception being that ASCE did not

distinguish between recommended values for total damping based on direction. Future work is needed to analyze these conclusions for other turbines with varying rotor sizes and dynamic characteristics.

Acknowledgements

The authors gratefully acknowledge Northeastern University and National Science Foundation Grant CMMI-1234560 for supporting this research.

Notation

a	=	Axial induction factor
a′	=	Tangential induction factor
C_D	=	Drag coefficient
C_L	=	Lift coefficient
c	=	Blade chord length
c_{ST}	=	Structural damping coefficient
c_{AD}	=	Aerodynamic damping coefficient
k	=	Lateral stiffness at the hub for equivalent single degree of freedom wind tower
F_x	=	Aerodynamic force at the hub in the fore-aft direction
F_y	=	Aerodynamic force at the hub in the side-to-side direction
m	=	Effective mass at the hub for equivalent single degree of freedom wind tower
N_b	=	Number of blades
r	=	Radial distance along the blade measured with respect to the blade root
TSR	=	Tip speed ratio, velocity of the blade tip with respect to V_w
V_{rel}	=	Velocity of the wind relative to the blade
V_w	=	Upstream wind velocity in the fore-aft direction
V_x	=	Wind velocity at the rotor in the fore-aft direction
V_y	=	Wind velocity at the rotor in the side-to-side direction

α	=	Angle of attack, the angle between V_{rel} and the blade chord
β	=	Blade pitch, the angle between the blade chord and the rotor plane
γ_i	=	The azimuth angle of the i^{th} blade
$\zeta_{AD,x}$	=	Aerodynamic damping ratio in the fore-aft direction
$\zeta_{AD,y}$	=	Aerodynamic damping ratio in the side-to-side direction
ρ	=	Air density
ϕ	=	The angle between V_{rel} and the rotor plane
Ω	=	Rotational speed of the rotor

References

American Society of Civil Engineers (ASCE), (2011). "Recommended Practice for Compliance of Large Land-based Wind Turbine Support Structures." ASCE/AWEA RP2011.

American Society of Civil Engineers (ASCE), (2010). "Minimum Design Loads for Buildings and Other Structures." (ASCE/SEI 7-10).

Bazeos, N. (2002). "Static, Seismic and Stability Analyses of a Prototype Wind Turbine Steel Tower." *Engineering Structures*, 24(8), 1015–1025.

Chopra, A.K. (2011). "Dynamics of Structures: Theory and Applications to Earthquake Engineering." Pearson/Prentice Hall, 4th Ed, Upper Saddle River, NJ.

Department of Energy (DOE), (2012). "Installed Wind Capacity." <http://www.windpoweringamerica.gov> (Jul. 9, 2013).

Federal Emergency Management Agency (FEMA), (2005). "Improvement of Nonlinear Static Seismic Analysis Procedures." FEMA-440, Washington (DC).

Garrad, A.D. (1990). "Forces and Dynamics of Horizontal Axes Wind Turbines." In: Freris LL." Wind Energy Conversion Systems". Prentice-Hall, New York, NY, 119-142.

Glauert, H. (1976). "Airplane Propellers." In Div. L, Aerodynamic Theory. Springer, Berlin.

Hansen, M.H., Thomsen, K., Fuglsang, P. (2006). "Two Methods for Estimating Aero-elastic Damping of Operational Wind Turbine Modes from Experiments." *Wind Energy*, 9(2), 179-191.

IEC (2005). "Wind Turbines – Part 1: Design Requirements," 3rd Edition. IEC 61400-1:2005-08. IEC, Geneva, Switzerland.

Kuhn, M. (2001). "Dynamics and Design Optimisation of Offshore Wind Energy Conversion Systems." Ph.D. thesis, DUWIND Delft University Wind Energy Research Institute, Delft, the Netherlands.

Lavassas, I., Nikolaidis, G., Zervas, P., Efthimiou, E., Doudoumis, I., Baniotopoulos, C.C. (2003). "Analysis and Design of the Prototype of a Steel 1-MW Wind Turbine Tower." *Engineering Structures*, 25(8), 1097–1106.

Malcolm, D.J., Hansen, A.C. (2002). "WindPACT Turbine Rotor Design Study: June 2000 - June 2002." NREL/SR-500-32495. Golden, CO, National Renewable Energy Laboratory.

Manwell, J.F., McGowan, J.G., Roger, A.L. (2002). "Wind Energy Explained: Theory, Design and Application." John Wiley and Sons Ltd., United Kingdom.

Nuta, E,. Christopoulos, C,. Packer, J.A. (2011). "Methodology for Seismic Risk Assessment for Tubular Steel Wind Turbine Towers: Application to Canadian Seismic Environment." *Canadian Journal of Civil Engineering*, 38(3), 293-304.

National Wind Technology Center (NWTC), (2013). "Computer-Aided Engineering Tools (FAST by Jason Jonkman, Ph.D)." <http://wind.nrel.gov/designcodes/simulators/fast> (Jul. 12, 2013).

Petersen, J.T., Madsen, H.A., Bjork, A., Enevoldsen, P., Ganander, H., Winkelaar, D. (1998). "Prediction of Dynamic Loads and Induced Vibrations in Stall." *Technical Report Technical Report Riso-R-1045(EN)*, Riso National Laboratory, Roskilde, Denmark.

Prowell, I., Veletzos, M., Elgamal, A., Restrepo, J. (2009). "Experimental and Numerical Seismic Response of a 65 kW Wind Turbine." *Journal of Earthquake Engineering*, 13(8), 1172-1190.

Prowell, I. (2011). "An Experimental and Numerical Study of Wind Turbine Seismic Behavior." PhD Dissertation, University of California, San Diego, CA.

Salzmann, C. D., Tempel, J. (2005). "Aerodynamic Damping in the Design of Support Structures for Offshore Wind Turbines." *Proc. of the Offshore Wind Energy Conference*, Copenhagen, Denmark.

Simiu, E. (2011). "Design of Buildings for Wind: A Guide for ASCE 7-10 Standard Users and Designers of Special Structures." John Wiley & Sons, Inc., 2nd Edition, Hoboken, New Jersey, NJ.

Thomsen, K., Peterson, J.T., Nim, E. (2000). "A Method for Determination of Damping for Edgewise Blade Vibrations," *Wind Energy*, 3(4), 233-246.

World Wind Energy Association (WWEA), (2013). "2012: Half-year Report." <http://www.wwindea.org> (Jul. 9, 2013).

World Wind Energy Association (WWEA), (2012). "2011: Report." <http://www.wwindea.org> (Jul. 9, 2013).

Witcher, D. (2005). "Seismic Analysis of Wind Turbines in the Time Domain." *Wind Energy*, 8(1), 81-91.

462 Xiong, L., Xianmin, Z., Gangqiang, L., Yan, C., Zhiquan, Y. (2010). "Dynamic Response Analysis of the
463 Rotating Blade of Horizontal Axis Wind Turbine." *Wind Engineering*, 35(5), 543-560.

Table 1. Specifications of the 1.5-MW baseline HAWT.

Power output	1.5 MW
Hub Height	84 m
Rotor Diameter	70 m
Number of Blades	3
Max Rotational Speed	20 rpm
Cut in wind speed	5 m/s
Cut out wind speed	25 m/s
Nacelle Mass	51 Ton
Hub Mass	15 Ton
Tower Mass	123 Ton
Rotor Mass	12 Ton
Active Pitch Control	Yes

Table
Click here to download Table: Table2.docx

Table 2. Features for each of the seven analyses conducted in FAST for comparison with predictions from the closed-form solution for the 1.5-MW baseline HAWT.

Analysis Number	Wind Shear[a]	Rotor	Yaw Error	Shaft Tilt[b]	Pre-cone[b]
1	$\alpha = 1/7$	Flexible	0°	-5°	-5°
2	None	Flexible	0°	0°	0°
3	$\alpha = 1/7$	Rigid	0°	0°	0°
4	None	Rigid	5°	0°	0°
5	None	Rigid	0°	-5°	0°
6	None	Rigid	0°	0°	-5°
7	None	Rigid	0°	0°	0°

[a]Wind shear based on power law. The exponent $\alpha = 1/7$ for open terrain (Simiu 2011).
[b]See FAST manual (NWTC 2013) for definition. Negative 5° is the prescribed value for the 1.5-MW baseline turbine.

Table
Click here to download Table: Table3.docx

Table 3. Characteristics of the seven ground motions considered in the seismic analysis.

Earthquake	Record ID	Magnitude	PGA (g)	S_a (g) T = 2.5 s $\xi = 5\%$
Landers	LSDSP000	7.5	0.17	0.04
Loma Prieta	LPSTG000	7.1	0.51	0.15
Loma Prieta	LPGIL067	7.1	0.36	0.06
Loma Prieta	LPLOB000	7.1	0.44	0.03
Loma Prieta	LPAND270	7.1	0.24	0.04
Morgan Hill	MHG06090	6.1	0.29	0.51
Northridge	NRORR360	6.8	0.51	0.18

Figure
Click here to download Figure: Fig1.pdf

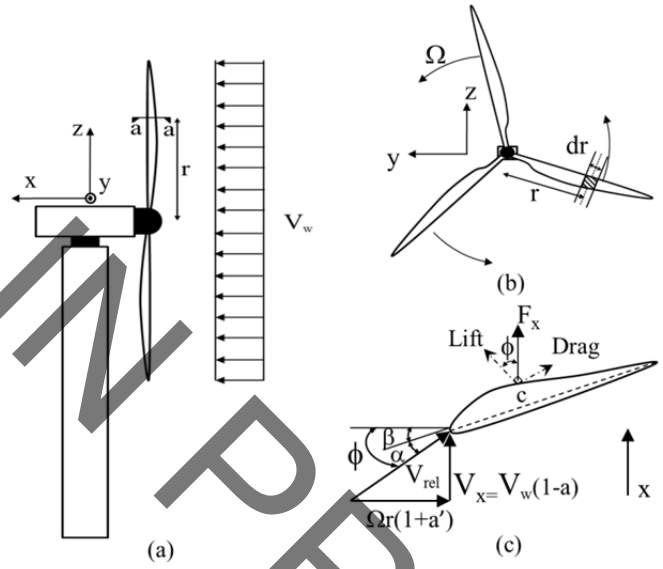

Figure
Click here to download Figure: Fig2.pdf

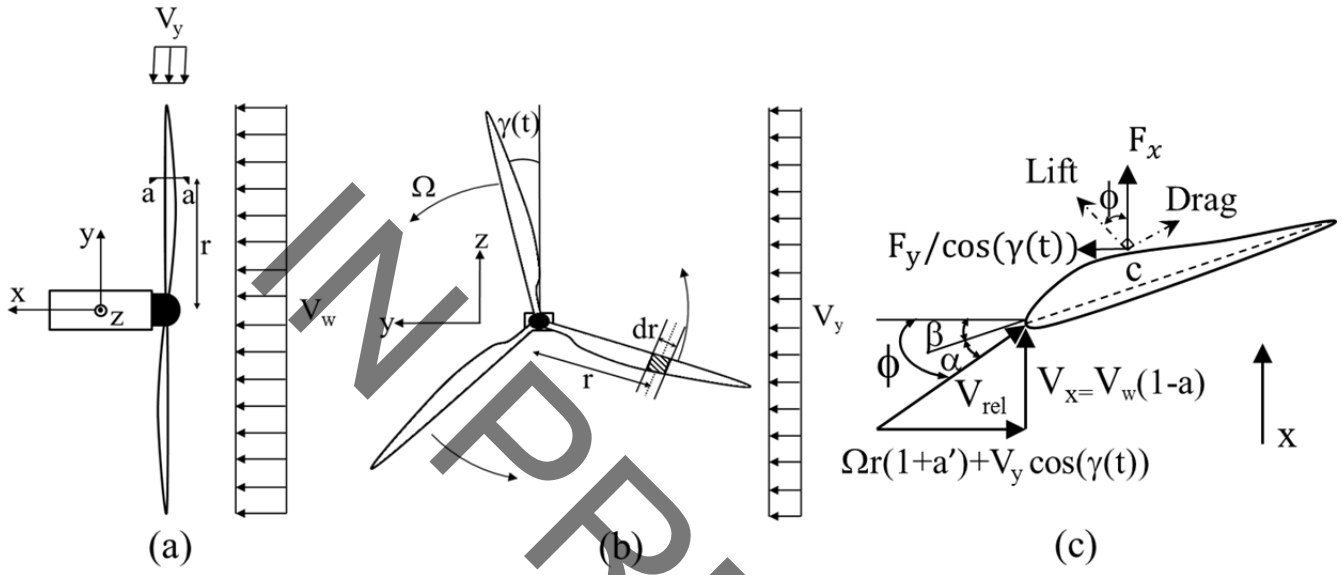

Figure
Click here to download Figure: Fig3.pdf

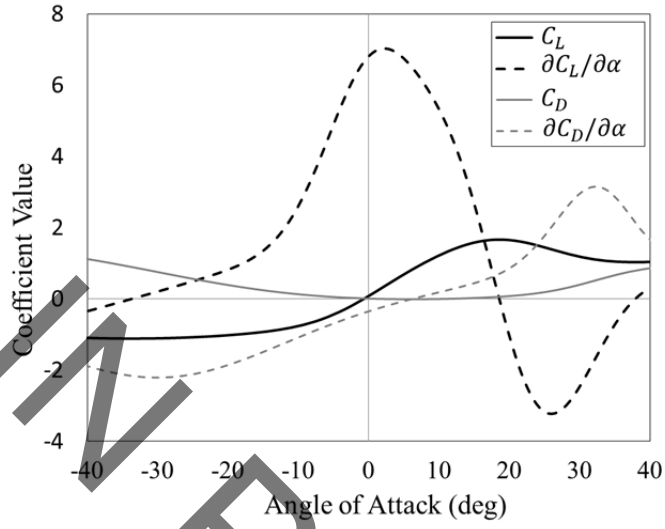

Figure
Click here to download Figure: Fig4.pdf

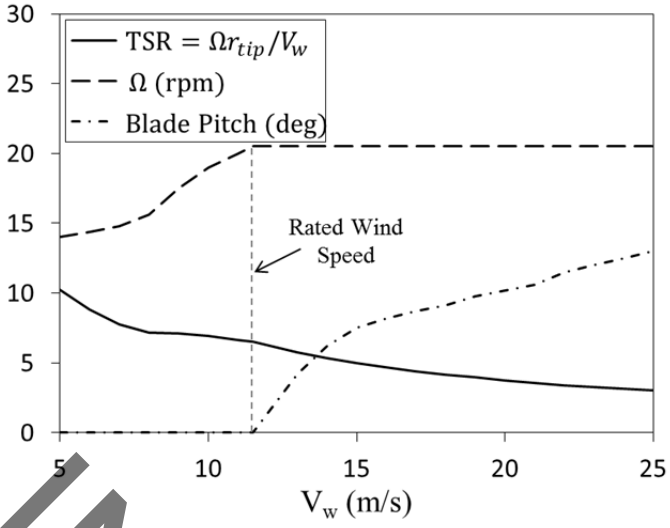

Figure
Click here to download Figure: Fig5.pdf

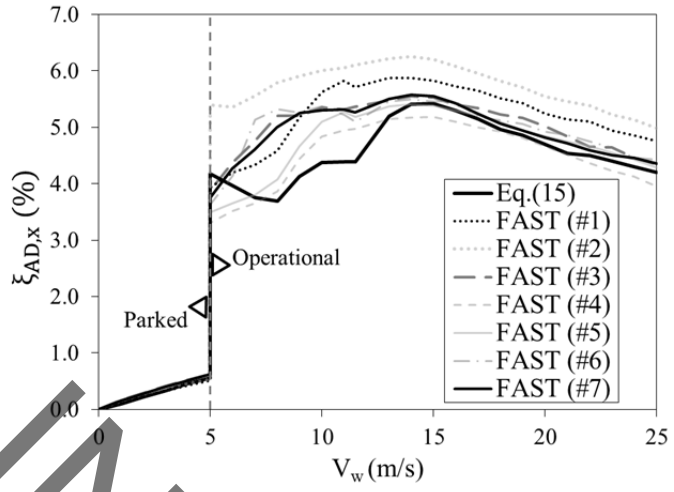

Figure
Click here to download Figure: Fig6.pdf

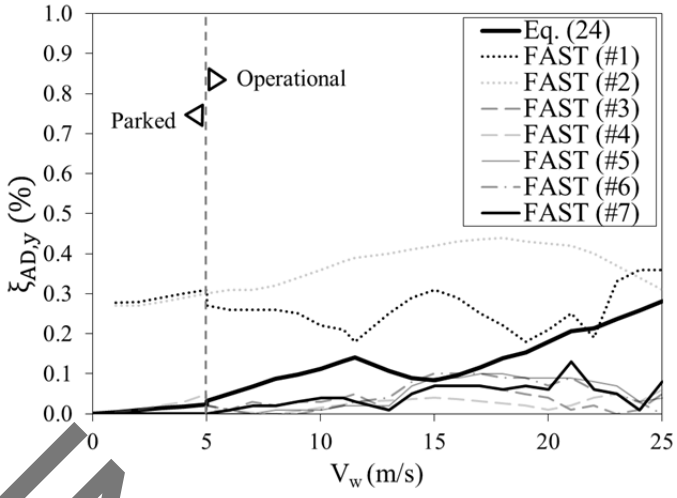

Figure
Click here to download Figure: Fig7.pdf

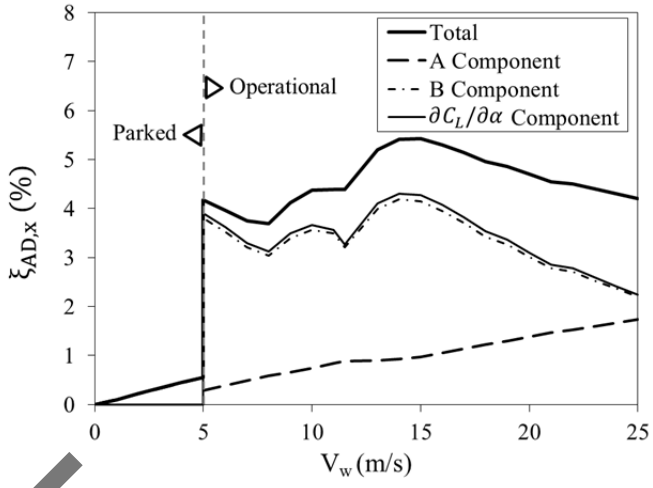

Figure
Click here to download Figure: Fig8.pdf

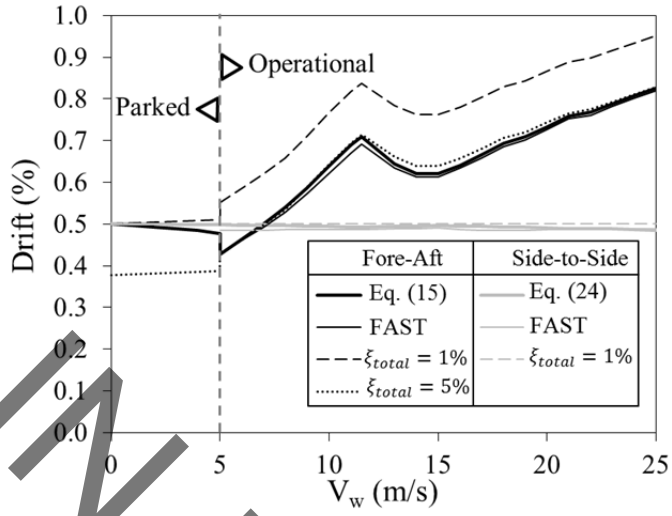

Fig. 1. Schematic representation indicating coordinate axes and variables for (a) a HAWT in elevation view, (b) a HAWT rotor in elevation view and (c) blade cross-section a-a.

Fig. 2. Schematic representation indicating coordinate axes and variables for the derivation of aerodynamic damping in the side-to-side direction for (a) a HAWT in plan view, (b) a HAWT rotor in elevation view and (c) blade cross-section a-a.

Fig. 3. Characteristics of the blade cross-section for the 1.5-MW baseline HAWT.

Fig. 4. Values of rotor speed Ω, blade pitch and tip speed ratio (TSR) versus wind speed for operational conditions between cut-in (5 m/s) and cut-out (25 m/s) for the 1.5-MW baseline turbine.

Fig. 5. Aerodynamic damping in the fore-aft direction during parked and operational conditions for the 1.5-MW baseline HAWT.

Fig. 6. Aerodynamic damping in the side-to-side direction during parked and operational conditions for the 1.5-MW baseline HAWT.

Fig. 7. Total aerodynamic damping and three of its components in the fore-aft direction during parked and operational conditions for the 1.5-MW baseline HAWT.

Fig. 8. Median spectral drift during parked and operational conditions for a dynamic model of the 1.5-MW baseline HAWT model subjected simultaneously to seismic loading and aerodynamic thrust on the rotor in the fore-aft direction. Results provided in the fore-aft and side-to-side directions for total damping calculated based on (1) the closed-form solution (2) FAST and (3) a constant value.